

# INFLATIONARY COSMOLOGY: FROM THEORY TO OBSERVATIONS

J. Alberto Vázquez <sup>1,2</sup>, Luis, E. Padilla <sup>2</sup>, Tonatiuh Matos <sup>2</sup>

## ABSTRACT

The main aim of this paper is to provide a qualitative introduction to the cosmic inflation and its relationship with current cosmological observations. The inflationary model solves many of the fundamental problems that challenge the Standard Big Bang cosmology i.e. Flatness, Horizon and Monopole problem, and additionally provides an explanation for the initial conditions observed throughout the Large-Scale Structure of the Universe, such as galaxies. In this review we describe the general solutions carry out by a single scalar field. Then with the use of current surveys, we show the constraints imposed on the inflationary parameters  $(n_s, r)$  which allow us to make the connection between theoretical and observational cosmology. In this way, with the latest results, it is possible to choose or at least to constrain the right inflationary model, parameterised by a single scalar field potential  $V(\phi)$ .

*Key Words:* cosmology: cosmological parameters — cosmology: observations — cosmology: inflation

## 1. INTRODUCTION

The Standard Big Bang (SBB) cosmology is currently the most accepted model describing the central features of the observed Universe. The big bang model, with the addition of dark matter and dark energy components, has been successfully proved on cosmological levels. For instance, measurements of the abundance of primordial elements and numerical simulations of structure formation of galaxies and galaxy clusters are in good agreement with astronomical observations (Kolb & Turner 1994; Tegmark et al. 2001; Springel et al. 2005). Also, the SBB model predicts the temperature fluctuations observed in the Cosmic Microwave Background radiation (CMB) with a high degree of accuracy: inhomogeneities of about one part in one hundred thousand (Komatsu et al. 2011; Planck 2015-XVI). These results, amongst many others, are the great success of the SBB cosmology. Nevertheless, when we have a closer look at different scales observations seem to present certain inconsistencies or unexplained features in contrast with expected by the theory.

<sup>1</sup>Instituto de Ciencias Físicas, Universidad Nacional Autónoma de México, Apdo. Postal 48-3, 62251 Cuernavaca, Morelos, México.

<sup>2</sup>Departamento de Física, Centro de Investigación y de Estudios Avanzados del IPN, México.

Some of these unsatisfactory aspects led to the emergence of the inflationary model (Guth 1981; Linde 1982, 1983; Albrecht & Steinhardt 1982).

In this work, we briefly present some of the relevant shortcomings the standard cosmology is dealing with, and a short review is carried out about the scalar fields as a promising solution. Moreover, it is shown that an inflationary single-field model can be completely described by providing its potential form  $V(\phi)$ . Based on the slow-roll approximation it is found that certain parameters, those that allow us to make the connexion with observations, are given by the amplitude of density perturbations  $\delta_H$ , the scalar spectral index  $n_s$  and the tensor-to-scalar ratio  $r$ . Finally, the theoretical predictions for different scalar field potentials are shown and compared with current observational data on the phase-space parameter  $n_s - r$ , therefore pinning down the number of candidates and making predictions about the shape of  $V(\phi)$ .

## 2. THE COSMOLOGICAL MODEL

To avoid long calculations and make this article accessible to young scientists, many technical details have been omitted or oversimplified; we encourage the reader to check out the vast amount of literature about the inflationary theory (Linde 1990; Kolb & Turner 1994; Liddle 1999; Liddle & Lyth 2000; Dodelson 2003).

Before starting with the theoretical description, let us consider some assumptions about the SBB model is built on (Coles & Lucchin 1995):

1) The physical laws at the present time can be extrapolated further back in time and be considered as valid in the early Universe. In this context, gravity is described by the theory of General Relativity, up to the Plank era.

2) The cosmological principle holds: “There do not exist preferred places in the Universe”. That is, the geometrical properties of the Universe at the largest-scales are based on the homogeneity and isotropy, both of them encoded on the Friedmann-Robertson-Walker (FRW) metric

$$ds^2 = -dt^2 + a^2(t) \left[ \frac{dr^2}{1 - kr^2} + r^2 (d\theta^2 + \sin^2\theta d\phi^2) \right], \quad (1)$$

where  $(t, r, \theta, \phi)$  describe the time-polar coordinates; the spatial curvature is given by the constant  $k$ , and the cosmic scale-factor  $a(t)$  parameterises the relative expansion of the Universe; commonly normalized to today’s value  $a(t_0) = 1$ . Hereafter we use natural units  $c = \hbar = 1$ , where the Planck mass  $m_{Pl}$  is related to the gravitational constant  $G$  through  $G \equiv m_{Pl}^{-2}$ .

3) On small scales, the anisotropic Universe is well described by a linear expansion of the metric around the FRW background:

$$g_{\mu\nu}(\mathbf{x}, t) = g_{\mu\nu}^{FRW}(\mathbf{x}, t) + h_{\mu\nu}(\mathbf{x}, t). \quad (2)$$

To describe the general properties of the Universe, we assume its dynamics is governed by a source treated as a perfect fluid with pressure  $p(t)$  and energy density  $\rho(t)$ . Both quantities often related via an equation-of-state with the form of  $p = p(\rho)$ . Some of the well studied cases are

$$\begin{aligned} p &= \frac{\rho}{3} && \text{Radiation,} \\ p &= 0 && \text{Dust,} \\ p &= -\rho && \text{Cosmological constant } \Lambda. \end{aligned} \quad (3)$$

The Einstein equations for these kind of constituents, and the FRW metric, are given by:

the **Friedmann equation**

$$H^2 \equiv \left( \frac{\dot{a}}{a} \right)^2 = \frac{8\pi}{3m_{Pl}^2} \rho - \frac{k}{a^2}, \quad (4)$$

the **acceleration equation**

$$\frac{\ddot{a}}{a} = -\frac{4\pi}{3m_{Pl}^2}(\rho + 3p), \quad (5)$$

and the energy conservation described by the **fluid equation**

$$\dot{\rho} + 3H(\rho + p) = 0, \quad (6)$$

where overdots indicate time derivative, and  $H$  defines the *Hubble parameter*. Notice that we could get the acceleration equation by time-deriving (4) and using (6), therefore only two of them are independent equations. Table 1 displays the solutions for the Friedmann and fluid equations with different components of the Universe.

From Eqn. (4) it can be seen that for a particular Hubble parameter there exists an energy density for which the universe may be spatially flat ( $k = 0$ ). This is known as the *critical density*  $\rho_c$  and is given by

$$\rho_c(t) = \frac{3m_{Pl}^2 H^2}{8\pi}, \quad (7)$$

where  $\rho_c$  is a function of time due to the presence of  $H$ . In particular, its current value is denoted by  $\rho_{c,0} = 1.87840 h^2 \times 10^{-26} \text{ kg m}^{-3}$ , or in terms of more convenient units taking into account large scales in the Universe,  $\rho_{c,0} = 2.775 h^{-1} \times 10^{11} M_\odot / (h^{-1} \text{ Mpc})^3$  (Planck 2015-XIII); with the solar mass denoted by  $M_\odot = 1.988 \times 10^{33} \text{ g}$  and  $h$  parameterises the present value of the Hubble parameter

$$H_0 = 100h \text{ km s}^{-1} \text{ Mpc}^{-1} = \frac{h}{3000} \text{ Mpc}^{-1}. \quad (8)$$

TABLE 1

Constituents of the universe and their behaviour: density evolution  $\rho(a)$ , scale factor  $a(t)$ , Hubble parameter  $H(t)$ .

component	$\rho_i(a)$	$a(t)$	$H(t)$
radiation	$\propto a^{-4}$	$\propto t^{1/2}$	$1/(2t)$
matter	$\propto a^{-3}$	$\propto t^{2/3}$	$2/(3t)$
cosmological constant	$\propto a^0$	$\propto \exp(\sqrt{\frac{\Lambda}{3}}t)$	const

The latest value of the Hubble parameter measured by the *Hubble Space Telescope* is quoted to be (Riess et al. 2016):

$$H_0 = 70.0_{-8,0}^{+12,0} \text{ kms}^{-1}\text{Mpc}^{-1}. \quad (9)$$

At the largest scales an useful quantity to measure is the ratio of the energy density to the critical density defining the *density parameter*  $\Omega_i \equiv \rho_i/\rho_c$ . The subscript  $i$  labels different constituents of the Universe such as radiation or matter. The Friedmann equation (4) can then be written in such a way to relate the total density parameter and the curvature of the Universe as

$$\Omega - 1 = \frac{k}{a^2 H^2}. \quad (10)$$

Thus the correspondence between the total density content  $\Omega$  and the space-time curvature for different  $k$  values is:

- Open Universe :  $0 < \Omega < 1 : k < 0 : \rho < \rho_c$ .
- Flat Universe :  $\Omega = 1 : k = 0 : \rho = \rho_c$ .
- Closed Universe:  $\Omega > 1 : k > 0 : \rho > \rho_c$ .

Current cosmological observations, based on the standard model, suggest the present value of  $\Omega$  is (McCoy 2014)

$$\Omega_0 = 1.00 \pm 0.002, \quad (11)$$

that is, the present Universe is nearly flat.

### 2.1. Shortcomings of the model

Once the equations that describe the Universe are known, then we need to incorporate the components of the cosmos, i.e. baryonic matter, radiation, dark matter and dark energy. This section presents some of the shortcoming the standard old cosmology is facing of, to then introduce the concept of Inflationary cosmology as a possible explanation to these issues.

#### Flatness problem

Notice that  $\Omega = 1$  is a special case of equation (10). If the Universe was perfectly flat at the earliest epochs, then it remained so for all time. Nevertheless a flat geometry is an unstable critical situation, that is, even a tiny deviation from it would cause that  $\Omega$  evolved quite differently and very quickly the Universe would have become more curved. This can be seen as a consequence due to  $aH$  is a decreasing function of time during radiation or matter domination epoch observed on the behaviour for each component, given in Table 1, then

$$\begin{aligned} |\Omega - 1| &\propto t && \text{during radiation domination,} \\ |\Omega - 1| &\propto t^{2/3} && \text{during dust domination.} \end{aligned}$$

Since the present age of the Universe is estimated to be  $t_0 \simeq 13.80 \pm 0.04$  Gyrs (Ast. parameters 2016), from the above equation we can deduce the required value of  $|\Omega - 1|$  at different times in order to obtain the correct spatial-geometry at the present time  $|\Omega_0 - 1|$ . For instance, let us consider some particular epochs in a nearly flat universe,

- At Decoupling time ( $t \simeq 10^{13}$  sec), we need that  $|\Omega - 1| \leq 10^{-3}$ .
- At Nucleosynthesis time ( $t \simeq 1$  sec), we need that  $|\Omega - 1| \leq 10^{-16}$ .
- At the Planck epoch ( $t \simeq 10^{-43}$  sec), we need that  $|\Omega - 1| \leq 10^{-64}$ .

Because there is no reason to prefer a Universe with critical density, hence  $|\Omega - 1|$  should not necessarily be exactly zero. Consequently, at early times  $|\Omega - 1|$  have to be fine-tuned extremely close to zero in order to reach its actual observed value.

### Horizon problem

The horizon problem is one of the most important problems in the Big Bang model, as it refers to the communication between different regions of the Universe. Bearing in that mind the existence of the Big Bang, the age of the Universe is a finite quantity and hence even light should have only travelled a finite distance by all this time.

According to the standard cosmology, photons decoupled from the rest of the components at temperatures about  $T_{dec} \approx 0.3 \text{ eV}$  at redshift  $z_{dec} \approx 1100$  (*decoupling time*), from this time on photons free-streamed and travelled basically uninterrupted until reach us, giving rise to the region known as the Observable Universe. This spherical surface, at which decoupling process occurred, is called *surface of last scattering*. The primordial photons are responsible for the CMB radiation observed today, then looking at its fluctuations is analogous of taking a picture of the universe at that time ( $t_{dec} \approx 380,000$  yrs old), see Figure 1.

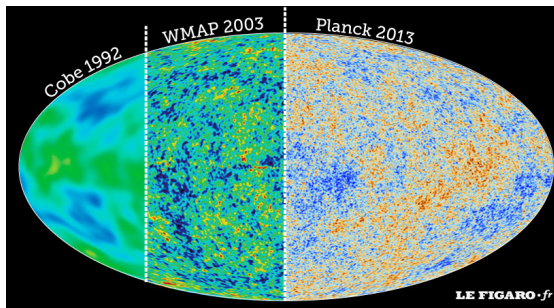


Fig. 1. Temperature fluctuations observed in the CMB using COBE-WMAP-Planck data (Gold et al. 2011; Planck 2015-XI,-)

Figure 1 shows light seen in all directions of the sky, these photons randomly distributed have nearly the same temperature  $T_0 = 2.725$  K plus small fluctuations (about one part in one hundred thousand) (Ast. parameters 2016; Planck 2015-XIII). As we have already pointed out being at the same temperature is a property of thermal equilibrium. Observations are therefore easily explained if different regions of the sky had been able to interact and moved towards thermal equilibrium. In other words, the isotropy observed in the CMB might imply that the radiation was homogeneous and isotropic within regions located on the last scattering surface. Oddly, the comoving horizon right before photons decoupled was significantly smaller than the corresponding horizon observed today. This means that photons coming from regions of the sky separated by more than the horizon scale at last scattering, typically about  $2^\circ$ , would not have been able to interact and established thermal equilibrium before decoupling. A simple calculation displays that at decoupling time the comoving horizon was  $90 h^{-1}$  Mpc and would be stretched up to  $2998 h^{-1}$  Mpc at present time. Then, the volume ratio provides that the microwave background should have consisted of about  $\sim 10^5$  causally disconnected regions (McCoy 2014). Therefore, the Big Bang model by itself does not offer an explanation on why temperatures seen in opposite directions of the sky are so accurately the same; the homogeneity must have been part of the initial conditions?

On the other hand, the microwave background is not perfectly isotropic, but instead exhibits small fluctuations as detected by, initially the Cosmic Background Explorer satellite (COBE) (Smooth et al. 1992), then with improved measurements by the Wilkinson Microwave Anisotropy Probe (WMAP) (Hinshaw et al. 2009; Larson et al. 2011) and nowadays with the Planck satellite (Planck 2016). These tiny irregularities are thought to be the ‘seeds’ that grew up until become the structure nowadays observed in the Universe.

### Monopole problem

Following the line to find out the simplest theory to describe the Universe, several models in particle physics were suggested in order to unified three of the four forces presented in the Standard Model of Particle Physics (SM): strong force, described by the group  $SU(3)$ , weak and electro-magnetic force, with an associated group  $SU(2) \otimes U(1)$ . These classes of theories are called *Grand Unified Theories (GUT)* (Georgi & Glashow 1974). An important point to mention in favour of GUT, is that they are the only ones that predict the equality electron-proton charge magnitude. Also, there are good reasons to believe the origin of *baryon asymmetry* might have been generated on the GUTs (Kolb & Turner 1983).

Basically, these kind of theories assert that in the early stages of the Universe ( $t \sim 10^{-43}$  sec), at highly extreme temperatures ( $T_{GUT} \sim 10^{32}$  K), existed a unified or *symmetric phase* described by a group  $G$ . As the Universe temperature dropped off, it went through different phase transitions until reach the matter particles such as electrons, protons, neutrons. When a phase transition happens its symmetry is broken and thus the symmetry group changes by itself, for instance:

- GUT transition:

$$G \rightarrow SU(3) \otimes SU(2) \otimes U(1).$$

- Electroweak transition:

$$SU(3) \otimes SU(2) \otimes U(1) \rightarrow SU(3) \otimes U(1).$$

The phase transitions have plenty of implications. One of the most important is the *topological defects* production which depends on the type of symmetry breaking and the spatial dimension (Vilenkin & Shellard 2000), some of them are:

- Monopoles (zero dimensional).
- Strings (one dimensional).
- Domain Walls (two dimensional).
- Textures (three dimensional).

Monopoles are therefore expected to emerge as a consequence of unification models. Besides that, from particle physics models there are not theoretical constraints on the mass a monopole should carry. However, from LHC constraints and grand unification theories, the mass of the monopole could be  $4 \times 10^3 - 10^{16}$  GeV (Mermod 2013). Hence, based on their non-relativistic character, a crude calculation predicts an extremely high abundance at present time (Coles & Lucchin 1995; Ambrosio 2002)

$$\Omega_M \simeq 10^{16}.$$

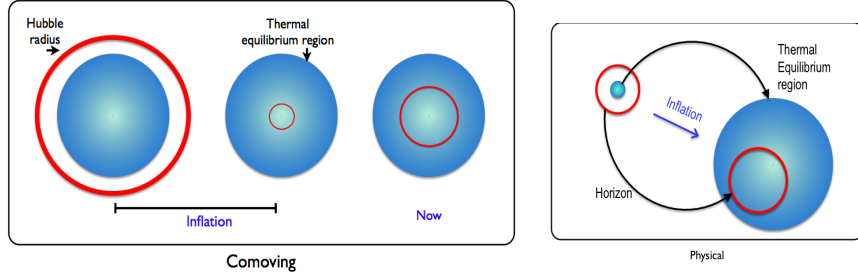


Fig. 2. Left: Schematic behaviour of the comoving Hubble radius during the inflationary period. Right: Physical evolution of the observable universe during the inflationary period.

According to this prediction, the Universe would be dominated by magnetic monopoles in contrast with current observations: no one has found anyone yet.

### 3. COSMOLOGICAL INFLATION

The inflationary model offers the most elegant way so far proposed to solve the problems of the standard big bang and therefore to understand why the universe is so remarkably in agreement with the standard cosmology. It does not replace the Big Bang model, but rather it is considered as an ‘auxiliary patch’ which occurred at the earliest stages without disturbing any of its successes.

*Inflation* is defined as the epoch in the early Universe in which the scale factor is exponentially expanded in just a fraction of a second:

$$\text{INFLATION} \iff \ddot{a} > 0 \quad (12)$$

$$\iff \frac{d}{dt} \left( \frac{1}{aH} \right) < 0. \quad (13)$$

The last term corresponds to the comoving Hubble length  $1/(aH)$  which is interpreted as the observable Universe becoming smaller during inflation. This process allows our observable region to lay down within a region that was inside the Hubble radius at the beginning of inflation. In Liddle (1999) words “is something similar to zooming in on a small region of the initial universe”, see Figure 2.

From the acceleration equation (5) the condition for inflation, in terms of the material required to drive the expansion, is

$$\ddot{a} > 0 \iff (\rho + 3p) < 0. \quad (14)$$



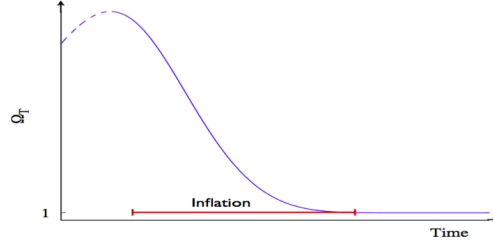


Fig. 3. Evolution of the density parameter  $\Omega$ , during the inflationary period.  $\Omega$  is driven towards unity, rather than away from it.

Because in standard physics it is always postulated  $\rho$  as a positive quantity, and hence in order to satisfy the acceleration condition is necessary for the overall pressure to have

$$\text{INFLATION} \iff p < -\rho/3. \quad (15)$$

Nonetheless, neither a radiation nor a matter component satisfies such condition. Let us postpone for a bit the problem of finding a candidate which may satisfy this inflationary condition.

### 3.1. Solution for the Big Bang Problems

If this brief period of accelerated expansion occurred, then it is possible that the aforementioned problems be solved.

#### Flatness problem

A typical solution is a Universe with a cosmological constant  $\Lambda$ , which can be interpreted as a perfect fluid with equation of state  $p = -\rho$ . Having this condition, we observe from Table 1 that the universe is exponentially expanded:

$$a(t) \propto \exp\left(\sqrt{\frac{\Lambda}{3}}t\right), \quad (16)$$

and the Hubble parameter  $H$  constant, then the condition (13) is naturally fulfilled. This epoch is called *de Sitter stage*. However, postulating a cosmological constant as a candidate to drive inflation might create more problems than solutions by itself, i.e. reheating process (Carroll 2001).

Let us look what happens when a general solution is considered. If somehow there was an accelerated expansion,  $1/(aH)$  tends to be smaller on time and hence, by the expression (10),  $\Omega$  is driven towards the unity rather than away from it. Then, we may ask ourselves by how much should  $1/(aH)$  decrease. If the inflationary period started at time  $t = t_i$  and ended up approximately at the beginning of the radiation dominated era ( $t = t_f$ ), then

$$|\Omega - 1|_{t=t_f} \sim 10^{-60},$$

and

$$\frac{|\Omega - 1|_{t=t_f}}{|\Omega - 1|_{t=t_i}} = \left(\frac{a_i}{a_f}\right)^2 \equiv e^{-2N}. \quad (17)$$

So, the required condition to reproduce the value of  $\Omega_0$  measured today is that inflation lasted for at least  $N \equiv \ln a \gtrsim 60$ , then  $\Omega$  will be extraordinarily close to one that we still observe it today. In this sense, inflation magnifies the curvature radius of the universe, so locally the universe seems to be flat with great precision, Figure 3.

### Horizon problem

As we have already seen, during inflation the universe expands drastically and there is a reduction in the comoving Hubble length. This allowed a tiny region located inside the Hubble radius to evolve and constitute our present observable Universe. Fluctuations were hence stretched outside of the horizon during inflation and re-entered the horizon in the late Universe, see Figure 2. Scales that were outside the horizon at CMB-decoupling were in fact inside the horizon before inflation. The region of space corresponding to the observable universe therefore was in thermal equilibrium before inflation and the uniformity of the CMB is essentially explained.

### Monopole problem

The monopole problem was initially the motivation to develop the inflationary cosmology (Guth 1997). During the inflationary epoch, the Universe led to a dramatic expansion over which the density of the unwanted particles were diluted away. Generating enough expansion, the dilution made sure the particles stayed completely out of the observable Universe making pretty difficult to localise even a single monopole.

## 4. SINGLE-FIELD INFLATION

Throughout the literature there exists a broad diversity of models that have been suggested to carry out the process (Liddle & Lyth 2000; Olive 1990; Lyth & Riotto 1999). In this section we present the scalar fields as good candidates to drive inflation and explain how relate theoretical predictions to observable quantities. Here, we limit ourselves to models based on general gravity, i.e. derived from the Einstein-Hilbert action, and single-field models described by a homogeneous slow-roll scalar field  $\phi$ . Nevertheless, in section 5 we provide a very brief introduction to several scalar fields, as a possibility

to generate the inflationary process.

Inflation relies on the existence of an early epoch in the Universe dominated by a very different form of energy; remember the requirement of the unusual property of a negative pressure. Such condition can be satisfied by a single scalar field (spin-0 particle). The scalar field which drives the Universe to an inflationary epoch is often termed as the *inflaton field*.

Let us consider a scalar field minimally coupled to gravity, with an arbitrary potential  $V(\phi)$  and Lagrangian density  $\mathcal{L}$  specified by

$$S = \int d^4x \sqrt{-g} \mathcal{L} = \int d^4x \sqrt{-g} \left[ \frac{1}{2} \partial_\mu \phi \partial^\mu \phi - V(\phi) \right]. \quad (18)$$

The energy-momentum tensor corresponding to this field is given by

$$T_{\mu\nu} = \partial_\mu \phi \partial_\nu \phi - g_{\mu\nu} \mathcal{L}. \quad (19)$$

In the same way as the perfect fluid treatment, the energy density  $\rho_\phi$  and pressure density  $p_\phi$  in the FRW metric are found to be

$$T_{00} = \rho_\phi = \frac{1}{2} \dot{\phi}^2 + V(\phi) + \frac{(\nabla \phi)^2}{2a^2}, \quad (20)$$

$$T_{ii} = p_\phi = \frac{1}{2} \dot{\phi}^2 - V(\phi) - \frac{(\nabla \phi)^2}{6a^2}. \quad (21)$$

Considering a homogeneous field, its corresponding equation of state is

$$w = \frac{p_\phi}{\rho_\phi} = \frac{\frac{1}{2} \dot{\phi}^2 - V(\phi)}{\frac{1}{2} \dot{\phi}^2 + V(\phi)}. \quad (22)$$

We can now split the inflaton field as

$$\phi(\mathbf{x}, t) = \phi_0(t) + \delta\phi(\mathbf{x}, t), \quad (23)$$

where  $\phi_0$  is considered a classical field, that is, the mean value of the inflaton on the homogeneous and isotropic state, whereas  $\delta\phi(\mathbf{x}, t)$  describes the quantum fluctuations around  $\phi_0$ .

The evolution equation for the background field  $\phi_0$  is given by

$$\ddot{\phi}_0 + 3H\dot{\phi}_0 = -V'(\phi_0), \quad (24)$$

and moreover, the Friedmann equation (4) with negligible curvature becomes

$$H^2 = \frac{8\pi}{3m_{Pl}^2} \left[ \frac{1}{2} \dot{\phi}_0^2 + V(\phi_0) \right], \quad (25)$$

where we have used primes as derivatives with respect to the scalar field  $\phi_0$ .

From the structure of the effective energy density and pressure, the acceleration equation (5) becomes,

$$\frac{\ddot{a}}{a} = -\frac{8\pi}{3m_{Pl}^2} \left( \dot{\phi}_0^2 - V(\phi_0) \right). \quad (26)$$

Therefore, the inflationary condition to be satisfied is  $\dot{\phi}_0^2 < V(\phi_0)$ , which is easily fulfilled with a suitably flat potential. Now on we shall omit the subscript ‘0’ by convenience.

#### 4.1. *Slow-roll approximation*

As we have noted, a period of accelerated expansion can be created by the cosmological constant ( $\Lambda$ ) and hence solve the aforementioned problems. After a brief period of time, inflation must end up and its energy being converted into conventional matter/radiation, this process is called *reheating*. In a Universe dominated by a cosmological constant the reheating process is seen as  $\Lambda$  decaying into conventional particles, however claiming that  $\Lambda$  is able to decay is still a naive way to face the problem. On the other hand, scalar fields have the property to behave like a *dynamical cosmological constant*. Based on this approach, it is useful to suggest a scalar field model starting with a nearly flat potential, i.e. initially satisfies the *first slow-roll* condition  $\dot{\phi}^2 \ll V(\phi)$ . This condition may not necessarily be fulfilled for a long time, but to avoid this problem, a second *slow-roll* condition is defined as  $|\ddot{\phi}| \ll |V_{,\phi}|$  or equivalently  $|\ddot{\phi}| \ll 3H|\dot{\phi}|$ . In this case the scalar field is slowly rolling down its potential and by obvious reasons such approximation is called *slow-roll* (Liddle & Lyth 1992; Liddle et al. 1994). The equations of motion (24) and (25), for slow-roll inflation, then become

$$3H\dot{\phi} \simeq -V'(\phi), \quad (27)$$

$$H^2 \simeq \frac{8\pi}{3m_{Pl}^2} V(\phi). \quad (28)$$

It is easily verifiable that the slow-roll approximation requires the slope and curvature of the potential to be small:  $V', V'' \ll V$ .

The inflationary process happens when the kinetic part of the inflaton field is subdominant over the potential field  $V(\phi)$ . When both quantities become comparable the inflationary period ends up giving rise finally to the reheating process, see Fig. 4.

It is now useful to introduce the potential *slow-roll parameters*  $\epsilon_v$  and  $\eta_v$  in the following way (Liddle & Lyth 1992; A. Riotto 2017)

$$\epsilon_v(\phi) \equiv \frac{m_{Pl}^2}{16\pi} \left( \frac{V'(\phi)}{V(\phi)} \right)^2, \quad (29)$$

$$\eta_v(\phi) \equiv \frac{m_{Pl}^2}{8\pi} \frac{V''(\phi)}{V(\phi)}. \quad (30)$$

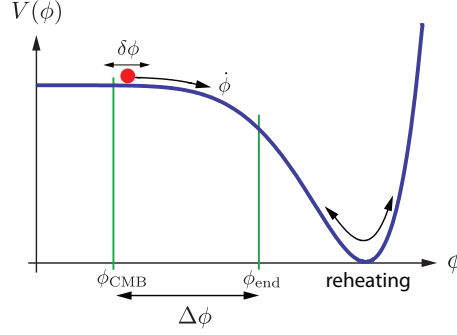


Fig. 4. Schematic inflationary process (Baumann & Peiris 2009).

Equations (27) and (28) are in agreement with the slow-roll approximation when the following conditions hold

$$\epsilon_v(\phi) \ll 1, \quad |\eta_v(\phi)| \ll 1.$$

These conditions are sufficient but not necessary, because the validity of the slow-roll approximations was a requirement in its derivation. The physical meaning of  $\epsilon_v(\phi)$  can be explicitly seen by expressing equation (12) in terms of  $\phi$ , then, the inflationary condition is equivalent to

$$\frac{\ddot{a}}{a} > 0 \implies \epsilon_v(\phi) < 1. \quad (31)$$

Hence, inflation concludes when the value  $\epsilon_v(\phi_{\text{end}}) = 1$  is approached.

Within these approximations, it is straightforward to find out the scale factor  $a$  between the beginning and the end of inflation. Because the size of the expansion is an enormous quantity, it is useful to compute it in terms of the  $e$ -fold number  $N$ , defined by

$$N \equiv \ln \frac{a(t_{\text{end}})}{a(t)} = \int_t^{t_e} H dt \simeq \frac{8\pi}{m_{Pl}^2} \int_{\phi_e}^{\phi} \frac{V}{V'} d\phi. \quad (32)$$

To give an estimate of the number of  $e$ -folds, let us assume that the evolution of the Universe can be split up into different epochs:

- Inflationary era: horizon crossing ( $k = aH$ )  $\rightarrow$  end of inflation  $a_{\text{end}}$ .
- Radiation era: reheating  $\rightarrow$  matter-radiation equality  $a_{\text{eq}}$ .
- Matter era:  $a_{\text{eq}} \rightarrow$  present  $a_0$ .

Assuming the transition between one era to another is instantaneous, then  $N(k) = \ln(a_k/a_0)$  can be easily computed with:

$$\frac{k}{a_0 H_0} = \frac{a_k H_k}{a_0 H_0} = \frac{a_k}{a_{\text{end}}} \frac{a_{\text{end}}}{a_{\text{reh}}} \frac{a_{\text{reh}}}{a_{\text{eq}}} \frac{a_{\text{eq}}}{a_0} \frac{H_k}{H_0}.$$

Then, one has (Liddle & Lyth 2000)

$$N(k) = 62 - \ln \frac{k}{a_0 H_0} - \ln \frac{10^{16} \text{GeV}}{V_k^{1/4}} + \ln \frac{V_k^{1/4}}{V_{end}} - \frac{1}{3} \ln \frac{V_{end}^{1/4}}{\rho_{reh}^{1/4}}.$$

The last three terms are small quantities related with energy scales during the inflationary process and usually can be ignored. The precise value for the second quantity depends on the model as well as the COBE normalisation, however it does not present any significant change to the total amount of  $e$ -folds. Thus, the value of total  $e$ -foldings is ranged from 50-70 (Lyth & Riotto 1999). Nevertheless, this value could change if a modification of the full history of the Universe is considered. For instance, thermal inflation can alter  $N$  up to a minimum value of  $N = 25$  (Lyth & Stewart 1995, 1996a).

As we noted, the parameters to describe inflation can be presented as a function of the scalar field potential. That is, specifying an inflationary model with a single scalar field is just selecting an inflationary potential  $V(\phi)$ . At this point, it is necessary to mention that these potentials are not chosen arbitrarily, but in fact, there is a whole line of research motivated by fundamental physics. For the purposes of this paper we will not delve into this subject, however, it will be understood that this potential is motivated by a fundamental theory. In order to exemplify our point, let us consider the following example.

The potential that describes a massive scalar field is given by:

$$V(\phi) = \frac{1}{2} m^2 \phi^2. \quad (33)$$

Considering the slow-roll approximation, equations (24) and (25) become:

$$\begin{aligned} 3H\dot{\phi} &= -m^2 \phi, \\ H^2 &= \frac{4\pi m^2 \phi^2}{3m_{pl}^2}. \end{aligned} \quad (34)$$

Thus, the dynamics of this type of model is described by

$$\begin{aligned} \phi(t) &= \phi_i - \frac{mm_{pl}}{\sqrt{12}\pi} t, \\ a(t) &= a_i \exp \left[ \sqrt{\frac{4\pi}{3}} \frac{m}{m_{pl}} \left( \phi_i t - \frac{mm_{pl}}{\sqrt{48}\pi} t^2 \right) \right], \end{aligned} \quad (35)$$

where  $\phi_i$  and  $a_i$  represent the initial conditions at a given initial time  $t = t_i$ . The slow-roll parameters for this particular potential are computed from equations (29) and (30)

$$\epsilon_v = \eta_v = \frac{m_{pl}^2}{4\pi} \frac{1}{\phi^2}, \quad (36)$$

that is, an inflationary epoch takes place whilst the condition  $|\phi| > m_{pl}/\sqrt{4\pi}$  is satisfied, and the total amount lapse during this accelerated period is encoded on the  $e$ -folds number

$$N_{tot} = \frac{2\pi}{m_{pl}^2} [\phi_i^2 - \phi_e^2]. \quad (37)$$

The steps shown before might, in principle, apply to any inflationary single-field model. That is, the general information we need to characterised cosmological inflation is specified by its potential.

#### 4.2. Cosmological Perturbations

Inflationary models have the merit that they do not only explain the homogeneity of the universe on large-scales, but also provide a theory for explaining the observed level of *anisotropy*. During the inflationary period, quantum fluctuations of the field were driven to scales much larger than the Hubble horizon. Then, in this process the fluctuations were frozen and turned into metric perturbations (Mukhanov & Chibisov 1997). Metric perturbations created during inflation can be described by two terms. The *scalar, or curvature*, perturbations are coupled with matter in the universe and form the initial “seeds” of structure observed in galaxies today. Although the *tensor perturbations* do not couple to matter, they are associated to the generation of primordial gravitational waves. As we shall see, scalar and tensor perturbations are seen as the important components to the CMB anisotropy (Hu & Dodelson 2002).

In a similar matter we have introduced the density parameter for large scales, on small scales we consider the *density contrast* defined by  $\delta \equiv \delta\rho/\rho$ . We now on assume *adiabatic initial conditions*, which require that matter and radiation perturbations are initially in perfect thermal equilibrium, and therefore the density contrast for different species in the Universe satisfy

$$\frac{1}{3}\delta_{\mathbf{k}b} = \frac{1}{3}\delta_{\mathbf{k}c} = \frac{1}{4}\delta_{\mathbf{k}\gamma} \left( = \frac{1}{4}\delta_{\mathbf{k}} \right). \quad (38)$$

The most general density perturbation is described by a linear combination of adiabatic perturbations as well as *isocurvature perturbations*, which the latter one plays an important role when more than one scalar field is considered (see next section and (Liddle & Lyth 2000)).

We introduce the *primordial curvature perturbation*  $\mathcal{R}_k(t)$ , which has the property to be constant within few Hubble times after the horizon exit given by  $k = aH$ . This value is called the *primordial value* and is related to the scalar field perturbation  $\delta\phi$  by

$$\mathcal{R}_k = - \left[ \frac{H}{\dot{\phi}} \delta\phi_k \right]_{k=aH}. \quad (39)$$

As already mentioned, if inflation provides an exponential expansion then the horizon remains practically constant while all other scales grow up. In this way, we can focus on the evolution of the quantum perturbations of the inflaton in a small region compared to the horizon. In this region it is possible to assume the space as locally flat and ignore the metric perturbations. Thus, working in the fourier space, the classical equation of motion for the perturbation part of  $\phi(\mathbf{x}, t)$  in (23) is

$$(\delta\phi_k)'' + 3H(\delta\phi_k)' + \left(\frac{k}{a}\right)^2 \delta\phi_k = 0, \quad (40)$$

where we have assumed  $\delta\phi$  is linear and neglect higher orders. This basically means that perturbations generated by vacuum fluctuations have uncorrelated Fourier modes, the signature of *Gaussian perturbations*.

The above equation can be rewritten as a harmonic oscillator equation with a variable frequency. If we now move to the quantum world and make the corresponding associations of operators to classical variables, the quantum dynamics will be determined by (Liddle & Lyth 2009)

$$\hat{\psi}_k(\eta) = \frac{\psi_k(\eta) \hat{a}(k) + \psi_k^*(\eta) \hat{a}^\dagger(-k)}{(2\pi)^3} \quad \text{with} \quad \psi_k(\eta) = -\frac{e^{-ik\eta}}{\sqrt{2k}} \frac{k\eta - i}{k\eta}, \quad (41)$$

where  $\hat{a}$  and  $\hat{a}^\dagger$  are the particle creation and annihilation operators,  $\eta$  is the proper time defined by  $\eta \equiv -1/aH$  and  $\psi \equiv a\delta\phi$ .

The inflationary process dilutes all possible particles existing before this period, and taking this into account so the ground state of the system is given by the vacuum. We notice that well after horizon exit,  $\eta \rightarrow 0$ ,  $\psi_k(\eta)$  approaches the value

$$\psi_k(\eta) = -\frac{i}{\sqrt{2k}} \frac{1}{k\eta}, \quad (42)$$

so that equation (41) is rewritten as

$$\hat{\psi}_k(\eta) = \psi_k(\eta) \frac{\hat{a}(k) - \hat{a}^\dagger(-k)}{(2\pi)^3}. \quad (43)$$

The temporal dependence of  $\hat{\psi}_k$  is now trivial and implies that once  $\psi_k(\eta)$  is measured after horizon exit, it will continue having a definite value. That this, quantum fluctuation become classical once they have crossed the horizon and therefore these quantum perturbations can be taken as the initial inhomogeneities that will later give rise to the structure formation. However these initial conditions will be slightly modified due to the amount of inflation remaining, once the  $k$ -scale has left the horizon.



Defining the spectrum of perturbations as

$$\begin{aligned}\langle \psi_k \psi_{k'}^* \rangle &= \frac{2\pi^2}{k^3} \mathcal{P}_\psi(k) \delta_D(\vec{k} - \vec{k}') \\ &= \frac{2\pi^2}{k^3} a^2 \mathcal{P}_\phi(k) \delta_D(\vec{k} - \vec{k}')\end{aligned}\quad (44)$$

where the Dirac's delta distribution  $\delta_D$  guarantees that modes relative to different wave-numbers are uncorrelated in order to preserve homogeneity. Evaluating the left hand side of the equation by a few Hubble times after the horizon exit,  $\eta = 1/aH_k$ , with the Hubble constant value  $H_k$  at the time the scale  $k$  has left the horizon yields to the spectrum

$$\mathcal{P}_\phi(k) = \left( \frac{H}{2\pi} \right)_{k=aH}^2. \quad (45)$$

From (39) and (45) the primordial curvature power spectrum  $\mathcal{P}_\mathcal{R}(k)$ , computed in terms of the scalar field spectrum  $\mathcal{P}_\phi(k)$  is given by

$$\begin{aligned}\mathcal{P}_\mathcal{R}(k) &= \left[ \left( \frac{H}{\dot{\phi}} \right)^2 \mathcal{P}_\phi(k) \right]_{k=aH} \\ &= \left[ \left( \frac{H}{\dot{\phi}} \right) \left( \frac{H}{2\pi} \right) \right]_{k=aH}^2.\end{aligned}\quad (46)$$

On the other hand, the creation of primordial gravitational waves corresponds to the tensor part of the metric perturbation  $h_{\mu\nu}$  in (2). In Fourier space, tensor perturbations  $h_{ij}$  can be expressed as the superposition of two polarisation modes

$$h_{ij} = h_+ e_{ij}^+ + h_\times e_{ij}^\times, \quad (47)$$

where  $+$ ,  $\times$  represent the longitudinal and transverse modes. From Einstein equations it is found that each amplitude  $h_+$  and  $h_\times$  behaves as a free scalar field in the sense that

$$\psi_{+, \times} \equiv \frac{m_{Pl}}{\sqrt{8}} h_{+, \times}. \quad (48)$$

Therefore, taking the results of the scalar perturbations, each  $h_{+, \times}$  has a spectrum  $\mathcal{P}_T$  given by

$$\mathcal{P}_T(k) = \frac{8}{m_{Pl}^2} \left( \frac{H}{2\pi} \right)_{k=aH}^2. \quad (49)$$

The canonical normalisation of the field  $\psi_{+, \times}$  was chosen such that the *tensor-to-scalar ratio* of the spectra is

$$r \equiv \frac{\mathcal{P}_T}{\mathcal{P}_\mathcal{R}} = 16\epsilon. \quad (50)$$

During the horizon exit,  $k = aH$ ,  $H$  and  $\dot{\phi}$  have tiny variations during few Hubble times. In this case, the scalar and tensor spectra are nearly scale invariant and therefore well approximated to a power law

$$\mathcal{P}_{\mathcal{R}}(k) = \mathcal{P}_{\mathcal{R}}(k_0) \left( \frac{k}{k_0} \right)^{n_s - 1}, \quad \mathcal{P}_T(k) = \mathcal{P}_T(k_0) \left( \frac{k}{k_0} \right)^{n_T}. \quad (51)$$

where the spectral indices are defined as

$$n_s - 1 \equiv \frac{d \ln \mathcal{P}_{\mathcal{R}}(k)}{d \ln k}, \quad n_T \equiv \frac{d \ln \mathcal{P}_T(k)}{d \ln k}. \quad (52)$$

A scale-invariant spectrum, called Harrison-Zel'dovich (HZ), has constant variance on all length scales and it is characterised by  $n_s = 1$ : small deviations from scale-invariance are also considered as a typical signature of the inflationary models. Then the spectral indices  $n_s$  and  $n_T$  can be expressed in terms of the slow-roll parameters  $\epsilon_v$  and  $\eta_v$ , to lowest order, as:

$$\begin{aligned} n_s - 1 &\simeq -6 \epsilon_v(\phi) + 2 \eta_v(\phi), \\ n_T &\simeq -2 \epsilon_v(\phi). \end{aligned} \quad (53)$$

These parameters are *not* completely independent each other, but the tensor spectral index is proportional to the tensor-to-scalar ratio  $r = -8n_T$ . This expression is the *first consistency relation* for slow-roll inflation. Hence, any inflationary model, to the lowest order in slow-roll, can be described in terms of three independent parameters: the amplitude of density perturbations  $\delta_H \sim \mathcal{P}_{\mathcal{R}}(k_0)^{1/2}$  ( $\approx 5 \times 10^{-5}$  initially measured by COBE satellite), the scalar spectral index  $n_s$ , and the tensor-to-scalar ratio  $r$ . If we require a more accurate description we have to consider higher-order effects, and then include parameters for describing the running of scalar ( $n_{s_{run}} \equiv dn_s/d \ln k$ ) and tensor ( $n_{T_{run}} \equiv dn_T/d \ln k$ ) index and higher order corrections.

An important point to emphasise is that  $\delta_H$ ,  $r$  and  $n_s$  are parameters that nowadays are tested from several observations. This allows us to compare theoretical predictions with observational data, for instance, those provided by the Cosmic Microwave Background radiation. In other words, future measurements of these parameters may probe or at least constrain the inflationary models and therefore the shape of the inflaton potential  $V(\phi)$ .

Let us get back to the massive scalar field example in equation (33). Inflation ends up when the condition  $\epsilon_v = 1$  is achieved, so  $\phi_{end} \simeq m_{pl}/\sqrt{2\pi}$ . As we pointed out before, we are interested in models with an  $e$ -fold number of about  $N_{tot} = 60$ , that is

$$\phi_i = \phi_{60} \simeq \sqrt{\frac{30}{\pi}} m_{pl}. \quad (54)$$

Finally, the spectral index and the tensor-to-scalar ratio for this potential are

$$n_s - 1 = -\frac{1}{30}, \quad r = \frac{2}{15}. \quad (55)$$

If the massive scalar field potential is the right inflationary model, current observations should favour the values  $n_s \approx 0.97$  and  $r \approx 0.1$ .

To determine the shape of the primordial power spectrum [Eqn. (46)] from cosmological observations, it is usual to assume a parameterised form for it. Even though the simplest assumption for the spectrum have a form of a power-law form given by Eqn. (51), there have been several studies regarding the shape of the primordial spectrum. Some of them based on physical models, some using observational data to constrain an a priori parameterisation, and others attempting a direct reconstruction from data (R. Hlozek et al. 2012; Vazquez et al. 2012a,b; Guo et al. 2011; Vazquez et al. 2013)

## 5. MULTI-FIELD INFLATION

Assuming that a single scalar field is responsible for inflation might be only an approximation, as the presence of multiple fields could drive this process too. In this section we show how the cosmological equations are modified when two scalar fields are responsible for driving inflation. (Byrnes and Wands 2006) The generalization to more than two fields can be easily obtained and described by (Gong 2016).

### 5.1. Background equation of motion

We consider a two-field inflationary model with canonical kinetic terms and its dynamics being described by an arbitrary interaction potential  $V(\phi, \psi)$ . As usual we assume the classical fields are homogeneous and evolve in a FLRW background. Thus, the background equation of motion for each scalar field and the Hubble parameter are

$$\ddot{\phi}_i + 3H\dot{\phi}_i + \frac{dV_i}{d|\phi_i|^2}\phi_i = 0, \quad (i = \phi, \psi), \quad (56a)$$

$$H^2 = \frac{8\pi}{3m_{Pl}^2} \left[ V + \frac{1}{2} (\dot{\phi}^2 + \dot{\psi}^2) \right], \quad (56b)$$

where  $V_i \equiv \partial V / \partial \phi_i$ . During inflation we adopt the slow-roll approximation for each field. This occurs always that the condition  $\epsilon_i, |\eta_{ij}| \ll 1$  is fulfilled;  $\epsilon_i$  and  $\eta_{ij}$  are now a new set of slow-roll parameters defined by

$$\epsilon_i = \frac{m_{Pl}^2}{16\pi} \left( \frac{V_i}{V} \right)^2, \quad \eta_{ij} = \frac{m_{Pl}^2}{8\pi} \left( \frac{V_{ij}}{V} \right). \quad (57)$$

The above equations are re-written in the slow-roll approximation as

$$\dot{\phi}_i \simeq -\frac{V_i}{3H} \left( 1 + \frac{1}{3} \delta_i^H \right), \quad H^2 \simeq \frac{8\pi}{3m_{Pl}^2} V \left( 1 + \frac{1}{3} \epsilon^H \right) \quad (58)$$

with  $\delta_i^H$  and  $\epsilon^H$  the new slow-roll parameters:

$$\delta_i^H = -\frac{\ddot{\phi}_i}{H\dot{\phi}_i}, \quad \epsilon^H = \epsilon_{\phi\phi} + \epsilon_{\psi\psi}. \quad (59)$$

### 5.2. Cosmological perturbations: The adiabatic and isocurvature perturbations

The equation of motion for the perturbed fields, in the spatially flat gauge, is described by

$$\ddot{\delta\phi}_i + 3H\dot{\delta\phi}_i + \sum_j \left[ V_{ij} - \frac{8\pi}{a^3 m_{Pl}^2} \frac{d}{dt} \left( \frac{a^3}{H} \dot{\phi}_i \dot{\phi}_j \right) \right] \delta\phi_j = 0. \quad (60)$$

On the largest scales ( $k \ll aH$ ) it is better to work on a rotating basis of the fields defined by the relation:

$$\begin{pmatrix} \delta\sigma \\ \delta s \end{pmatrix} = S^\dagger \begin{pmatrix} \delta\phi \\ \delta\psi \end{pmatrix}, \quad (61a)$$

where

$$S = \begin{pmatrix} \cos\theta & -\sin\theta \\ \sin\theta & \cos\theta \end{pmatrix}, \quad \tan\theta = \frac{\dot{\psi}}{\dot{\phi}} \simeq \pm \sqrt{\frac{\epsilon_\psi}{\epsilon_\phi}}. \quad (61b)$$

The field  $\sigma$  is parallel to the trajectory on the field space and it is usually called *adiabatic field*, whereas the field  $s$  is perpendicular and named the *entropy field*. If the background trajectory is curved then  $\delta\sigma$  and  $\delta s$  are correlated at Hubble exit, and therefore at this point the power spectrum and cross-correlation are described by the expressions:

$$P_{\sigma^*}(k) \simeq \left( \frac{H_*}{2\pi} \right)^2 (1 + (-2 + 6C)\epsilon - 2C\eta_{\sigma\sigma}), \quad (62a)$$

$$C_{\sigma s^*}(k) \simeq -2C\eta_{\sigma s} \left( \frac{H_*}{2\pi} \right)^2, \quad (62b)$$

$$P_{s^*}(k) \simeq \left( \frac{H_*}{2\pi} \right)^2 (1 + (-2 + 2C)\epsilon - 2C\eta_{ss}), \quad (62c)$$

where  $C \simeq 0.7296$ ,  $\epsilon \equiv \epsilon_{\sigma\sigma} + \epsilon_{ss}$  and  $\eta_{ij}$  ( $i, j = \sigma, s$ ) are slow-roll parameters defined in a similar way that Eq. (57), but now in terms of the new fields  $\sigma$  and  $s$ .

#### 5.2.1. Final power spectrum and spectral index

The curvature and isocurvature perturbations are usually defined as

$$R \equiv \frac{H}{\dot{\sigma}} \delta\sigma, \quad S = \frac{H}{\dot{\sigma}} \delta s. \quad (63)$$

In the slow-roll limit, on large scales, the evolution of curvature and isocurvature perturbations can be written using the formalism of transfer matrix:

$$\begin{pmatrix} R \\ S \end{pmatrix} = \begin{pmatrix} 1 & T_{RS} \\ 0 & T_{SS} \end{pmatrix} \begin{pmatrix} R \\ S \end{pmatrix}_*, \quad (64)$$

where

$$T_{SS}(t^*, t) = \exp\left(\int_{t^*}^t \beta H dt'\right), \quad T_{RS}(t^*, t) = \exp\left(\int_{t^*}^t \alpha T_{SS} H dt'\right), \quad (65)$$

and at linear order in slow-roll parameters

$$\alpha \simeq -2\eta_{\sigma s}, \quad \beta \simeq -2\epsilon + \eta_{\sigma\sigma} - \eta_{ss}, \quad (66)$$

where again  $\eta_{ij}$  is defined in a similar fashion than Eqs. (57) but in terms of the new fields  $\sigma$  and  $s$ .

On the other hand, the primordial curvature perturbation during a radiation-dominated era (some time after inflation ended) is given on large scales by

$$R = \Psi + \frac{H\delta\rho}{\rho}, \quad (67)$$

where  $\Psi$  is the gravitational potential. The conventional definition of the isocurvature perturbation for an  $i$ -specie is given relative to the radiation density by

$$S_i = H \left( \frac{\delta\rho_i}{\rho_i} - \frac{\delta\rho_\gamma}{\rho_\gamma} \right). \quad (68)$$

Then, at the beginning of the radiation-domination era we get the final power spectra

$$P_R \simeq P|_*(1 + \cot^2 \Delta), \quad (69a)$$

$$P_S = T_{SS}^2 P|_*, \quad (69b)$$

$$C_{RS} = T_{RS} T_{SS} P_R|_*, \quad (69c)$$

where at linear order in slow-roll parameters  $P|_*$  is

$$P|_* = \frac{1}{2\epsilon} \left( \frac{2H_*}{m_{pl}} \right)^2, \quad (70)$$

with  $\Delta$  the observable correlation angle defined at lower order as

$$\cos \Delta = \frac{T_{RS}}{\sqrt{1 + T_{RS}^2}}. \quad (71)$$

The final spectral index for each contribution, defined as  $n_x - 1 = d \ln P_x / d \ln k$ , at linear order in slow-roll parameters are

$$\begin{aligned} n_s - 1 &\simeq -(6 - 4 \cos^2 \Delta) \epsilon + 2 \sin^2 \Delta \eta_{\sigma\sigma}, \\ &\quad + 4 \sin \Delta \cos \Delta \eta_{\sigma s} + 2 \cos^2 \Delta \eta_{ss}, \end{aligned} \quad (72a)$$

$$n_C - 1 \simeq -2\epsilon + 2 \tan \Delta \eta_{\sigma s} + 2 \eta_{ss}, \quad (72b)$$

$$n_S - 1 \simeq -2\epsilon + 2 \eta_{ss}. \quad (72c)$$

Notice that we have left the subindex  $s$  in order to be consistent with the scalar spectral index defined in the single inflationary scenario.

Sometimes it is also common to parameterise the primordial adiabatic and entropy perturbations on super-horizon scales as power laws

$$P_R = A_r^2 \left( \frac{k}{k_0} \right)^{n_{ad1}-1} + A_s^2 \left( \frac{k}{k_0} \right)^{n_{ad2}-1}, \quad (73a)$$

$$C_{RS} = A_s B \left( \frac{k}{k_0} \right)^{n_{cor}-1}, \quad (73b)$$

$$P_s = B^2 \left( \frac{k}{k_0} \right)^{n_{iso}-1}, \quad (73c)$$

where at linear order  $n_{ad1} = -6\epsilon + 2\eta_{\sigma\sigma}$ ,  $n_{ad2} = 2n_C - n_S$ ,  $n_{cor} = n_C$ ,  $n_{iso} = n_S$ . We have that  $A_r^2$ ,  $A_s^2$  and  $B$  can be written in terms of the correlation angle as

$$A_r^2 = [P_R \sin^2 \Delta]_{k_0}, \quad A_s^2 = [P_R \cos^2 \Delta]_{k_0}, \quad (74a)$$

$$B^2 = [T_{SS}^2 P_R]_{k_0}, \quad (74b)$$

$A_r^2$  and  $A_s^2$  are the contributions of the adiabatic and entropy fields to the amplitude of the primordial adiabatic spectrum.

### 5.2.2. Gravitational waves

Given the fact that scalar and tensor perturbations are decoupled at linear order, gravitational waves at horizon crossing is the same than in the single-field case and the amplitude of gravitational waves remained frozen on large scales after Hubble exit during inflation. Therefore the tensor power spectrum and the spectral index are finally

$$P_T = P_{T*} \simeq 8 \left( \frac{H_*}{2\pi m_{pl}} \right)^2 (1 + 2(-1 + C)\epsilon), \quad (75)$$

$$n_T \simeq -2\epsilon \left[ 1 + \left( \frac{4}{3} + 4C \right) \epsilon + \left( \frac{2}{3} + 2C \right) \eta_{\sigma\sigma} \right], \quad (76)$$

The tensor-to-scalar ratio at Hubble exit is the same than in the single field case. However, at super-horizon scales, the curvature perturbations continue evolving as (69a). In this way the value of  $r$  some time after the end of inflation is

$$r \simeq 16\epsilon \sin^2 \Delta \left[ 1 - \left( \frac{4}{3} + 4C \right) \epsilon + \left( \frac{2}{3} + 2C \right) \eta_{\sigma\sigma} \right]. \quad (77)$$

We can observe from (50) that the single scalar field case works as an upper constraint on  $r$ .

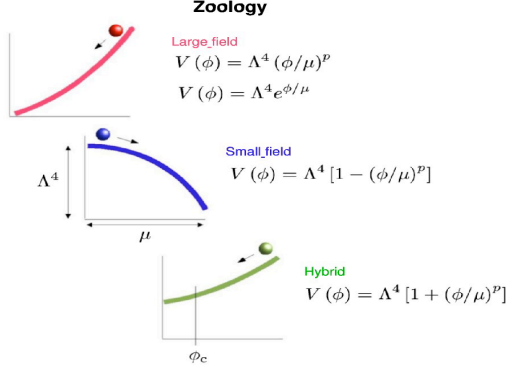


Fig. 5. Potential classification. From top to bottom: *large field*, *small field* and *hybrid potential* (Kinney 2004).

## 6. INFLATIONARY MODELS

We have seen that a single-field inflationary model could be described by the specification of the potential form  $V(\phi)$ . In this case the comparison of model predictions to CMB observations reduces to the following basic steps:

1. Given a scalar field potential  $V(\phi)$ , compute the slow roll parameters  $\epsilon_v(\phi)$  and  $\eta_v(\phi)$ .
2. Find out  $\phi_{end}$  given by  $\epsilon(\phi_{end}) = 1$ .
3. From equation (32), compute the field at about 60  $e$ -folds  $\phi_{60}$ .
4. Compute  $n_s$  and  $r$  as functions of  $\phi$ , and finally evaluate them at  $\phi = \phi_{60}$  which can be tested by the CMB data.

Different types of models are classified by the relationship among their slow-roll parameters  $\epsilon$  and  $\eta$ , which are reflected on different relations between  $n_s$  and  $r$ . Hence, an appropriate parameter space to show the diversity of models is well described by the  $n_s$ — $r$  plane.

### 6.1. Models

Even if we restrict the analysis to a single-field, the number of inflationary models available is enormous (Liddle & Lyth 2000; Lyth & Riotto 1999; Linde 2005). Then, it is convenient to classify different kinds of potentials following Kinney (2004). The classification is based on the behaviour of the potential during inflation. The three basic types are shown in Figure 5. *Large field*: the field is initially displaced from a stable minimum and evolves towards it. *Small field*: the field evolves away from an unstable maximum. *Hybrid*: the field evolves towards a minimum with vacuum energy different from zero.

A general single field potential can be written in terms of a *height*  $\Lambda$  and a *width*  $\mu$ , such as

$$V(\phi) = \Lambda^4 f\left(\frac{\phi}{\mu}\right). \quad (78)$$

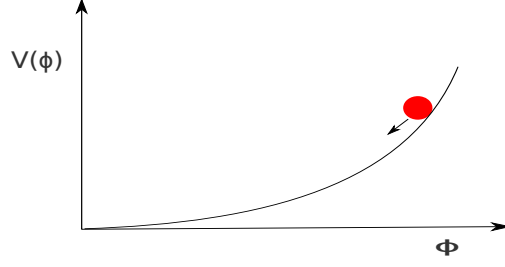


Fig. 6. Chaotic inflationary potential.

Different models have different forms for the function  $f$ .

### 6.2. Large-field models: $-\epsilon < \eta \leq \epsilon$

**Large field** models perhaps possess the simplest type of monomial potentials. These kind of potentials represent the *chaotic* inflationary scenarios (Linde 1983). The distinctive of these models is that the shape of the effective potential is not very important in detail. That is, a region of the Universe where the scalar field is usually situated at  $\phi \sim m_{\text{Pl}}$  from the minimum of its potential will automatically lead to inflation, see Figure 6. Such models are described by  $V''(\phi) > 0$  and  $-\epsilon < \eta \leq \epsilon$ .

A general set of large-field polynomial potentials can be written as

$$V(\phi) = \Lambda^4 \left( \frac{\phi}{\mu} \right)^p, \quad (79)$$

where it is enough to choose the exponent  $p > 1$  in order to specify a particular model. This model gives

$$\begin{aligned} n_s - 1 &= -\frac{2+p}{2N}, \\ r &= \frac{4p}{N}. \end{aligned} \quad (80)$$

In this case, gravitational waves can be sufficiently big to eventually be observed ( $r \gtrsim 0.1$ ). From the quadratic potential of equation (33), we obtain

$$\epsilon \simeq 0.008, \quad \eta \simeq 0.008, \quad n_s \simeq 0.97, \quad r \simeq 0.128 \quad (81)$$

In the high power limit the  $V \propto \phi^p$  predictions are the same as the exponential potential (La & Steinhardt 1999). Hence, a variant of this class of models is

$$V(\phi) = \Lambda^4 \exp(\phi/\mu). \quad (82)$$



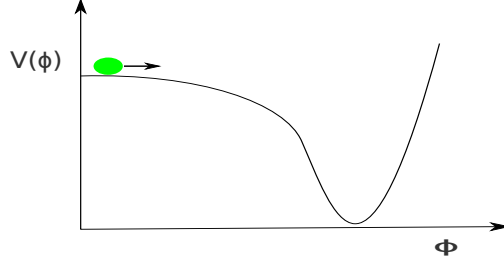


Fig. 7. New inflationary potential.

This type of potential is a rare case presented in inflation because its dynamics has an exact solution given by a power-law expansion. For this case the spectral index  $n_s$  is closely related to the tensor-to-scalar ratio  $r$ , as

$$\begin{aligned} n_s - 1 &= -\frac{m_{pl}^2}{8\pi\mu^2}, \\ r &= 8(1 - n_s), \end{aligned} \quad (83)$$

as we observe, the slow-roll parameters are explicitly independent of the  $e$ -fold number  $N$ .

### 6.3. Small-field models: $\eta < -\epsilon$

**Small field** models are typically described by potentials that arise naturally from spontaneous symmetry breaking, these type of models are also known as *new inflation* (Albrecht & Steinhardt 1982; Linde 1983). In this case, inflation takes place when the field is situated in a false vacuum state, very close to the top of the hill and rolls down to a stable minimum, see Figure 7. These models are typically characterized by  $V''(\phi) < 0$  and  $\eta < -\epsilon$ , usually  $\epsilon$  is closely zero (and hence the tensor amplitude). Small field potentials, can be written in the generic form as

$$V(\phi) = \Lambda^4 [1 - (\phi/\mu)^p], \quad (84)$$

where the exponent  $p$  differs from model to model.  $V(\phi)$  is usually considered as the lowest-order in a Taylor expansion from a more general potential. In the simplest case of spontaneous symmetry breaking with no special symmetries, the dominant term is the mass term,  $p = 2$ , hence the model gives

$$\begin{aligned} n_s - 1 &\simeq -\left(\frac{m_{Pl}}{\mu}\right)^2, \\ N &= \frac{4\pi\mu^2}{m_{pl}^2} \left[ \ln\left(\frac{\phi_{end}}{\phi_i}\right) - \frac{\phi_{end} - \phi_i}{2\mu^2} \right] \\ r &= 8(1 - n_s) \exp[-1 - N(1 - n_s)]. \end{aligned} \quad (85)$$

$$(86)$$

On the other hand,  $p > 2$  has a very different behavior. The scalar spectral index is

$$n_s - 1 = -\frac{2}{N} \left( \frac{p-1}{p-2} \right), \quad (87)$$

independent of  $(m_{Pl}/\mu)$ . In addition, the tensor-to-scalar ratio for this model is given by

$$r = 8 \left( \frac{\mu}{M_{pl}} \right)^{2p/(p-2)} \left( \frac{p}{2N(p-2)} \right)^{2(p-1)/(p-2)} \quad (88)$$

#### 6.4. Hybrid models: $0 < \epsilon < \eta$

The third class called **hybrid models** frequently include those that incorporate supersymmetry into inflation (Linde 1991; Copeland et al. 1994). In these models, the inflaton field  $\phi$  evolves towards a minimum of its potential, however the minimum has a vacuum energy  $V(\phi_{\min}) = \Lambda^4$  different to zero. In such cases, inflation continues forever unless an auxiliary field  $\psi$  is added to interact with  $\phi$  and ends inflation at some point  $\phi = \phi_c$ . Such models are well described by  $V''(\phi) > 0$  and  $0 < \epsilon < \eta$ , where  $V$  is the effective 1-field potential for the inflaton.

The generic potential for hybrid inflation, in a similar way to large field and small field models, are considered as

$$V(\phi) = \Lambda^4 [1 + (\phi/\mu)^p]. \quad (89)$$

For  $(\phi_N/\mu) \gg 1$  the behaviour of the large-field models is recovered. Besides that, when  $(\phi_N/\mu) \ll 1$  the dynamics is similar to small-field models, but now the field is evolving towards a dynamical fixed point rather than away from it. Because the presence of an auxiliary field the number of  $e$ -folds is

$$N(\phi) \simeq \left( \frac{p+1}{p+2} \right) \left[ \frac{1}{\eta(\phi_c)} - \frac{1}{\eta(\phi)} \right]. \quad (90)$$

For  $\phi \gg \phi_c$ ,  $N(\phi)$  approaches the value

$$N_{max} \equiv \left( \frac{p+1}{p+2} \right) \frac{1}{\eta(\phi_c)}. \quad (91)$$

In general

$$N = \frac{8\pi\mu^p}{pm_{pl}^2} \left[ \frac{\phi_{end}^{2-p} - \phi_i^{2-p}}{2-p} + \frac{\phi_{end}^2 - \phi_i^2}{2\mu^p} \right], \quad \text{for } p \neq 2 \quad (92)$$

$$N = \frac{8\pi\mu^p}{pm_{pl}^2} \left[ \ln \left( \frac{\phi_{end}}{\phi_i} \right) + \frac{\phi_{end}^2 - \phi_i^2}{2\mu^p} \right], \quad \text{for } p = 2 \quad (93)$$

and therefore, the spectral index is given by

$$n_s - 1 \simeq 2 \left( \frac{p+1}{p+2} \right) \frac{1}{N_{max} - N}.$$

As we can note, the power spectrum is *blue* ( $n_s > 1$ ) and besides that, the model presents a running of the spectral index

$$\frac{dn_s}{d \ln k} = -\frac{1}{2} \left( \frac{p+2}{p+1} \right) (n_s - 1)^2. \quad (94)$$

This parameter will be very useful for higher orders and more accurate constraints in future observations. For instance, the particular case  $p = 2$  and  $n_s = 1.2$ , the running obtained is  $dn_s/d \ln k = -0.05$  (Kinney & Riotto 1998).

### 6.5. Linear models: $\eta = -\epsilon$

Linear models,  $V(\phi) \propto \phi$ , are located on the limits between large field and small field models. They are represented by  $V''(\phi) = 0$  and  $\eta = -\epsilon$ . The spectral index and tensor-to-scalar ratio are given by

$$n_s - 1 = -\frac{6}{1 - 4N}, \quad r = \frac{16}{1 - 4N}. \quad (95)$$

### 6.6. Logarithmic inflation

There still remain several single-field models which cannot fit into this classification, for instance the logarithmic potentials (Barrow & Parsons 1995)

$$V(\phi) = V_0 [1 + (Cg^2/8\pi^2) \ln(\phi/\mu)]. \quad (96)$$

Typically they correspond to loop corrections in a supersymmetric theory, where  $C$  denotes the degrees of freedom coupled to the inflaton and  $g$  is a coupling constant. For this potential, the inflationary parameters are

$$\begin{aligned} n_s - 1 &\simeq -\frac{1}{N}, \\ r &\simeq \sqrt{\frac{1}{N} \frac{Cg^2}{16\pi}}. \end{aligned} \quad (97)$$

In this model, to end up inflation, an auxiliary field is needed, which is the main feature of hybrid models. However when it is plotted on the  $n_s$ — $r$  plane, is located into the small-field region.

### 6.7. Hybrid Natural Inflation

Hybrid Natural Inflation is particularly appealing because its origins lie in well motivated physics. The inflaton potential relevant to the inflationary era has the general form

$$V(\phi) = \Delta^4 (1 + a \cos(\frac{\phi}{f})), \quad (98)$$

where  $f$  is the symmetry breaking scale and  $a$  allows for more general inflationary phenomena that can readily accommodate the Planck results, and even

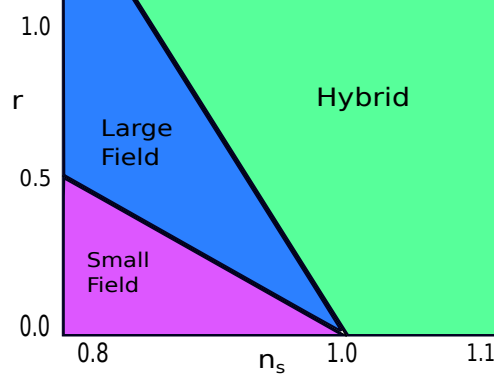


Fig. 8. Classification of the potentials in terms of  $n_s$  and  $r$  parameters.

allow for a low-scale of inflation. Here the inflaton,  $\phi$ , is a pseudo-Goldstone boson associated with a spontaneously broken global symmetry and is thus protected from large radiative corrections to its mass. Defining  $c_\phi$  and  $s_\phi$  by  $\cos(\frac{\phi}{f})$  and  $\sin(\frac{\phi}{f})$  respectively, we get

$$\epsilon = \frac{1}{16\pi} \left( \frac{a}{f} \right)^2 \frac{s_\phi^2}{(1 + a c_\phi)^2}, \quad (99)$$

$$\eta = -\frac{1}{8\pi} \left( \frac{a}{f^2} \right) \frac{c_\phi}{1 + a c_\phi}, \quad (100)$$

and the inflationary parameters are computed and constrained by Graham (2016).

The classification of inflationary models mentioned previously may be interpreted as an arbitrary one. Although, it is very useful because different types of models cover different regions of the  $(n_s, r)$  plane without overlapping, see Figure 8.

### 6.8. Hybrid waterfall inflation

A two-field inflationary scenario is an alternative case of the hybrid models studied in section 6.4. It occurs when the mass of the auxiliary field is smaller than the hubble parameter, i.e.  $V_{\psi\psi} \lesssim H$ . Once the inflaton acquires a critical value  $\phi_c$ , the auxiliary field starts evolving slowly and a period of inflation is produced during its dynamics, usually called as the *waterfall scenario*. An interesting result is the possibility to obtain a *red* power spectrum ( $n_s < 1$ ) depending on the amount of inflation produced during the waterfall period. As an example, let us consider two scalar fields with a potential like chaotic-hybrid :

$$V^t = \frac{\lambda}{4} \left[ \left( \frac{M^2}{\lambda} - \psi^2 \right)^2 + \frac{1}{2} m^2 \phi^2 + \frac{1}{2} g^2 \phi^2 \psi^2 \right], \quad (101)$$

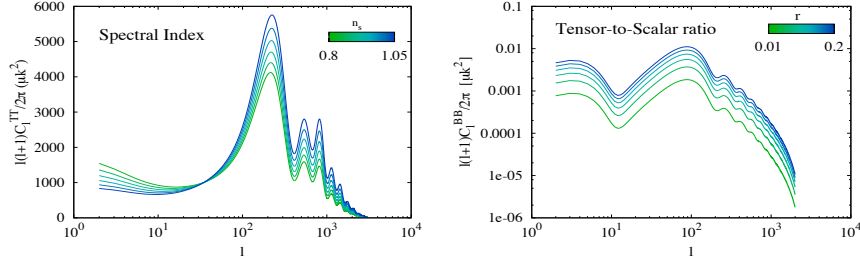


Fig. 9. Variations of the CMB scalar spectrum for different values of the spectral index  $n_s$  (left), and variations of the CMB tensor spectrum with respect to the tensor-to-scalar ratio  $r$  (right).

with  $M, m, \lambda$  constant values. In the typical hybrid models, it is expected that the *waterfall* field  $\psi$  remains a  $\psi = 0$  whilst the inflaton field  $\phi$  evolves generating inflation. Then, when  $\phi = \phi_c$  the minimum  $\psi = 0$  becomes unstable and the waterfall field rolls down to its true minimum, finishing up immediately with the inflationary era. However, if  $M^2 \lesssim H^2$  we obtain the waterfall period. Considering the limit  $g^2\psi^2/H^2 \ll m^2/H^2$  (i.e. the back-reaction of the waterfall field on the inflaton is small during inflation) and  $\psi^2/H^2 \ll M^2/\lambda H^2$  we obtain finally that (Abolhasani, Firouzjahi and Namjoo 2010)

$$n_s - 1 \simeq \frac{4M^2}{3H_0^2} \left( \frac{M^2}{9H_0^2} - r n_m \right) \quad (102)$$

where  $H_0$  is the value of the Hubble parameter at the moment of inflation and  $n_m = N_m - N_c$  is a measurement of the differences between the  $e$ -folds  $N_m$  when a given scale  $k$  left the horizon and the  $e$ -folds  $N_c$  when the waterfall transition starts. Then, for modes that left the horizon before the phase transition we have  $n_m < 0$  and  $n_s > 1$ , whereas for modes that left the horizon after a phase transition we have that  $n_m > 0$  and  $n_s$  can take any value.

## 7. OBSERVATIONAL RESULTS

How can observations constrain  $n_s$  and  $r$  in inflationary models? During several years many projects, at different scales, have been carried out in order to look for observational data to constrain cosmological models. That is, different models may imprint different behaviours over the CMB spectra, see Figure 9. Amongst many projects, they are: Cosmic Background Explorer (COBE), Wilkinson Microwave Anisotropy Probe (WMAP), Cosmic Background Imager observations (CBI), Balloon Observations of Millimetric Extra-galactic Radiation and Geophysics (BOOMERang), the Luminous Red Galaxy (LRG) subset DR7 of the Sloan Digital Sky Survey (SDSS), Baryon Acoustic Oscillations (BAO), Supernovae (SNe) data, Hubble Space Telescope

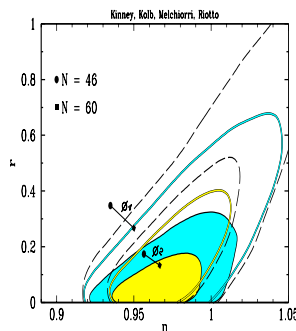


Fig. 10. WMAP3 only (open contours) and WMAP3+SDSS (filled contours) 2D posterior distributions on the phase space  $n_s$ - $r$ , for the potentials  $\phi^2$  and  $\phi^4$  by considering  $e$ -folds of  $N \sim 46$  and  $60$ . Coloured regions correspond to 68% and 95% CL (Kinney et al. 2006).

(HST) and recently the South Pole Telescope (SPT), the Atacama Cosmology Telescope (ACT) and the Planck Satellite. Below, we show some of the constraints for different types of inflationary potentials, by using current observational data (Mortonson et al. 2011). We stress that the results are shown on the phase space  $n_s - r$  and therefore our interest is mainly focussed on the case with no running,  $dn_s/d\ln k = 0$ .

Figure 10 displays marginalised 2D posterior distributions for  $n_s$  and  $r$  based on two data sets: WMAP3 by itself, and WMAP3 plus information from the LRG subset from SDSS (Kinney et al. 2006). Considering WMAP3 observations alone (open contours) the parameters are constrained such that  $0.94 < n_s < 1.04$  and  $r < 0.60$  (95% CL). Those models that present  $n_s < 0.9$  are therefore ruled out at high confidence level. The same is applied for models with  $n_s > 1.05$ . WMAP data by itself cannot lead to strong constraints because the existence of parameter degeneracies, like the well known geometrical degeneracy involving  $\Omega_m$ ,  $\Omega_\Lambda$  and  $\Omega_k$ . However, when it is combined with different types of datasets, together they increase the constraining power and might remove degeneracies. Once the SDSS data is included the limit of the gravitational wave amplitude and the spectral index constraints are reduced, that is, for WMAP3+SDSS (filled contours) the constraints on  $n_s$  and  $r$  are  $0.93 < n_s < 1.01$  and  $r < 0.31$ . Moreover, Figure 10 shows that the Harrison-Zel'dovich model:  $n_s = 1, r = 0, dn_s/d\ln k = 0$ , is still in good agreement with data. Similarly, for inflation driven by a massless self-interacting scalar field  $V(\phi) = \lambda\phi^4$ , the contours indicate that this potential with 60  $e$ -folds is still consistent with WMAP3 data at 95% CL, nevertheless ruled out by the combined datasets WMAP3+SDSS. The potential  $V(\phi) = m^2\phi^2/2$  is consistent with both data sets, with a preference to 60  $e$ -folds.

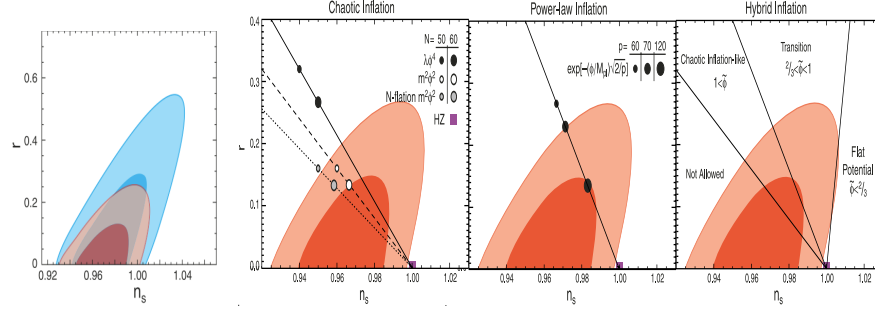


Fig. 11. Constraints on  $n_s$  and  $r$ . Left panel: WMAP5 results are coloured blue and WMAP5+BAO+SN red. Right panel: Constraints on large and hybrid models from the combined datasets WMAP5+BAO+SN. Coloured regions correspond to 68% and 95% CL (Komatsu 2009).

On the other hand, left panel of figure 11 shows limits imposed by WMAP5 data alone,  $r < 0.43$  (95% CL) while  $0.964 < n_s < 1.008$ . When BAO and SN data are added, the limits improve significantly to  $r < 0.22$  (95% CL) and  $0.953 < n_s < 0.983$  (Komatsu 2009). Right panel of figure 11 displays a summary for different potentials constraints by WMAP5+BAO+SN. The model  $V(\phi) = \lambda\phi^4$ , unlike WMAP3 constraints, is found to be located far away from the 95% CL, and therefore it is excluded by more than  $2\sigma$ . For inflation produced by a massive scalar field  $V(\phi) = (1/2)m^2\phi^2$ , the model with  $N = 50$  is situated outside the 68% CL, whereas with  $N = 60$  is at the boundary of the 68% CL. Therefore, this model is consistent with data within the 95% CL. The points represented by  $N$ -flation describe a model with many massive axion fields (Liddle 1998). For an exponential potential, it is observed that models with  $p < 60$  are mainly excluded. Models with  $60 < p < 70$  are roughly in the boundary of the 95% region, and  $p > 70$  are in agreement within the 95% CL. Some models with  $p \sim 120$  essentially lay out in the limit of the 68% CL.

The hybrid potentials, as already noted, can have different behaviours depending on the  $(\phi/\mu)$  value. The parameter space can be split into three different regions based on  $(\phi/\mu)$ . For  $\phi/\mu \ll 1$  the dynamics is similar to small fields and the dominant term lays in the region called “Flat Potential Regime”. For  $\phi/\mu \gg 1$  the results are similar to large field models and this region is called “Chaotic Inflation-like Regime”. The boundary,  $\phi/\mu \sim 1$  is named “Transition regime”. The different  $(\phi/\mu)$  values corresponding to their regions are shown in the right panel of Figure 11. Finally, the combined datasets WMAP5+BAO+SN ruled out the Harrison-Zel’dovich model by more than 95% CL.

Following the same line for inflationary models, we use the COSMOMC

package (Lewis & Bridle 2002) which allows us to perform the parameter estimation and to provide constraints for the  $n_s$  and  $r$  parameters given a dataset [we refer to Padilla et al. (2018) where the authors provided an introduction on Bayesian parameter inference and its applications to cosmology]. We assume a flat  $\Lambda$ CDM model specified by the following parameters: the physical baryon  $\Omega_b h^2$  and cold dark matter density  $\Omega_{DM} h^2$  relative to the critical density,  $\theta$  is  $100 \times$  the ratio of the sound horizon to angular diameter distance at last scattering surface and  $\tau$  denotes the optical depth at reionisation. To illustrate our point, we initially consider WMAP seven year data. We observe from Figure 12 that in order a model to be considered as a favourable candidate it has to predict a spectral index about  $n_s = 0.982^{+0.020}_{-0.019}$  and a tensor-to-scalar ratio  $r < 0.37$  (95% CL). When WMAP-7 is combined with different datasets, the constraints are tighten as it is shown by Larson et al. (2011).

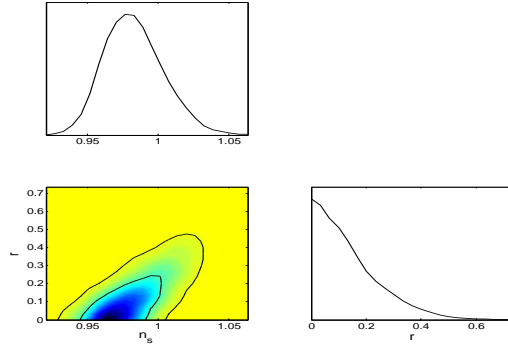


Fig. 12. 1D and 2D Marginalised probability constraints on  $n_s$  and  $r$  using only WMAP7 data. 2D constraints are plotted with  $1\sigma$  and  $2\sigma$  confidence contours

Two recent experiments have placed new constraints on the cosmological parameters: the Atacama Cosmology Telescope (ACT) Dunkley et al. (2010) and the South Pole Telescope (SPT) Keisler et al. (2011). Figure 13 shows the predicted values for a chaotic inflationary model with inflaton potential  $V(\phi) \propto \phi^p$  with 60 e-folds. We observe that models with  $p \geq 3$  are disfavored at more than 95% CL.

Figure 14 shows recent constrains given by Planck Colaboration (2015) in the  $n_s$  and  $r$  plane. Gray regions correspond to the Planck 2013 results, red regions added the contribution of the temperature power spectrum (TT) and the Planck polarization data in the low- $l$  likelihood (lowP) while blue regions added the temperature-polarization cross spectrum (TE) and the polarisation power spectrum (EE). Notice that the model that fit the best to the data corresponds to  $R^2$  inflation (Starobinsky 1980) and models  $V(\phi) \propto \phi^p$  with  $p \geq 3$  are discarded by data. Finally, the addition of BAO data and lensing is shown in Figure 15.



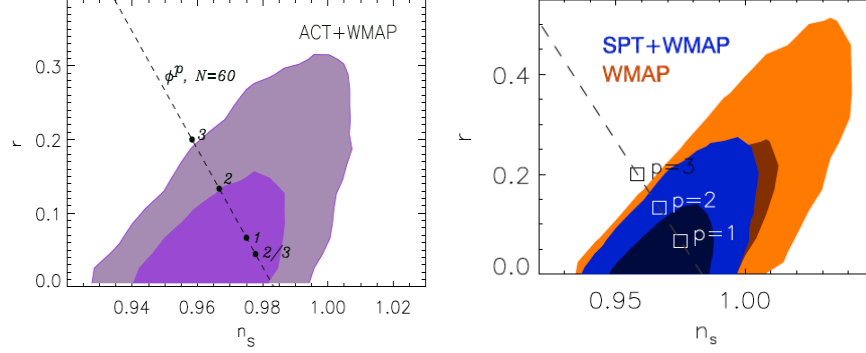


Fig. 13. Marginalized 2D probability distribution (68% and 95% CL) for the tensor-to-scalar ratio  $r$ , and the scalar spectral index  $n_s$  for ACT+WMAP (left panel) and SPT+WMAP (right panel) (Dunkley et al. 2010; Keisler et al. 2011).

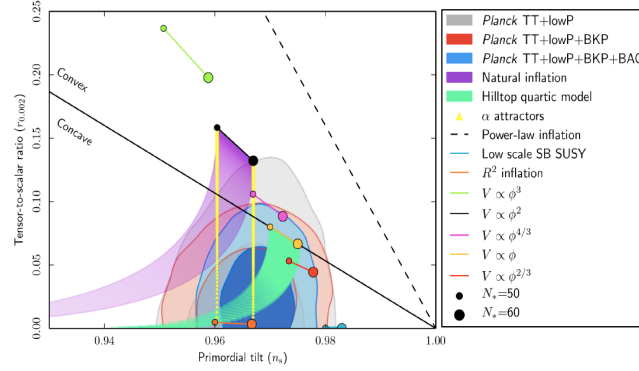


Fig. 14. 2D marginalised probability constraints on  $n_s$  and  $r$  for the most recent results of (Planck Collaboration 2015). 2D constraints are plotted with  $1\sigma$  and  $2\sigma$  confidence contours. Figure taken from Planck Collaboration (2015).

## 8. CONCLUSIONS

Considering the analysis presented here is complicated to prove that a given model is correct, since these could be just particular cases of more general models with several parameters involved. However, it is possible to eliminate models or at least give some constraints on their behaviour leading to a narrower range of study. Although we have presented some simple examples of potentials, the classification in small-field, large-field, and hybrid models is enough to cover the entire region of the  $n_s$ – $r$  plane as illustrated in Figure 8. Different versions of the three types of models predict qualitatively different scalar and tensor spectra, so it should be particularly easy to work on them apart.

We have seen that the favoured models are those with small  $r$  (for  $dn_s/d \ln k \sim$

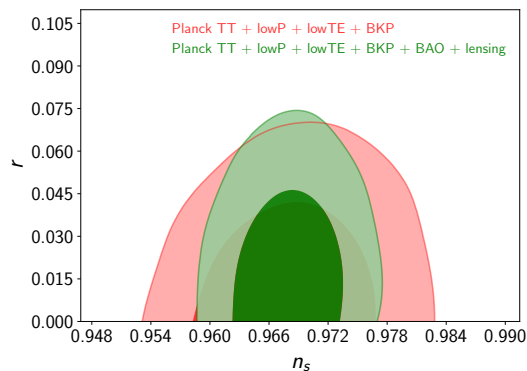


Fig. 15. 2D marginalised probability constraints on  $n_s$  and  $r$  for the most recent results of Planck dataset. 2D constraints are plotted with  $1\sigma$  and  $2\sigma$  confidence contours. Figure done by using the CosmoMC package.

0) and slightly *red* spectrum, hence models with *blue* power spectrum  $n_s > 1.0$  are inconsistent with the recent data. These simple but important constraints allow us to rule out the simplest models corresponding to hybrid inflation of the form  $V(\phi) = \Lambda^4(1 + (\mu/\phi)^p)$ . There still remain models with red spectra in the hybrid classification: inverted models and models with logarithmic potentials.

Table 2 summarises the constraints on the  $n_s$  and  $r$  parameters and its improvements through the years. Scale-invariant power spectrum  $n_s = 1$  is consistent within 95% CL with WMAP3 data and therefore not ruled out, however with WMAP5 data the HZ spectrum lays outside the 95% CL region, which indicates it is excluded considering the lowest order on the  $n_s, r$  parameters. When WMAP7 data is considered, scale-invariant spectrum is totally excluded by more than  $3\sigma$ , however the inclusion of extra parameters may weaken the constraints on the spectral index. When chaotic models  $V(\phi) \propto \phi^p$  are analysed with current data, it is found that quartic models ( $p = 4$ ) are ruled out, whilst models with  $p \geq 3$  are disfavoured at  $> 95\%$  CL. Moreover, the quadratic potential  $V(\phi) = 1/2m^2\phi^2$  is in agreement with all data sets presented here and therefore remains as a good candidate. Future surveys will provide a more accurate description of the universe and therefore narrow the number of candidates which might better explain the inflationary period.

## 9. ACKNOWLEDGMENTS

LEP was supported by CONACyT México.

## REFERENCES

- A. A. Abolhasani, H. Firouzjahi, and M. H. Namjoo, (2010), arXiv:1010.6292 [astro-ph.CO] .

TABLE 2  
SUMMARISE OF THE  $n_s$ ,  $r$  CONSTRAINTS FROM DIFFERENT  
MEASUREMENTS <sup>a</sup>.

Parameter	Limits	Data set
$n_s$ $r$	$0.9683 \pm 0.0059$ $< 0.0660$	Planck TT + lowP + lowTE + BKP + BAO + lensing
$n_s$ $r$	$0.9666 \pm 0.0062$ $< 0.103$	Planck TT+lowP
$n_s$ $r$	$0.9711 \pm 0.0099$ $< 0.17$	SPT+WMAP7+BAO+ $H_0$
$n_s$ $r$	$0.970 \pm 0.012$ $< 0.19$	ACT+WMAP7+BAO+ $H_0$
$n_s$ $r$	$0.973 \pm 0.014$ $< 0.24$	WMAP7 + BAO + $H_0$
$n_s$ $r$	$0.982^{+0.020}_{-0.019}$ $< 0.36$	WMAP7 ONLY
$n_s$ $r$	$0.968 \pm 0.015$ $< 0.22$	WMAP5+BAO+SN
$n_s$ $r$	$0.986 \pm 0.022$ $< 0.43$	WMAP5 ONLY
$n_s$ $r$	$0.97 \pm 0.04$ $< 0.31$	WMAP3 + SDSS
$n_s$ $r$	$0.99 \pm 0.05$ $< 0.60$	WMAP3 ONLY

<sup>a</sup>Peiris et al.2003; Kinney et al.2006; Komatsu et al.2009; Komatsu et al.2011; Dunkley et al. 2010; Keisler et al. 2011, Planckck

- Ade P. A. R. et al. Planck collaboration. Astron. Astrophys. 594, A20 (2016).  
arXiv:1502.02114
- Albrecht, A., and Steinhardt, P. J. 1982, Phys. Rev. Lett., 48, 1220
- Ambrosio, M., et al. 2002, Eur. Phys. J. C., 25, 511
- Astrophysical Constant and Parameters, <http://pdg.lbl.gov/2016/reviews/rpp2016-rev-astrophysical-constants.pdf>, revised December 2017
- Barrow, J. D., and Parsons, P. 1995, Phys. Rev. D, 52, 10
- Baumann, D., and Peiris, H. V. 2009, Adv. Sci. Lett., 2, 105
- C. D. McCoy, What Is the Horizon Problem?, november 2014
- Carroll, S. 2001, Living Rev. Relativity, 3
- Christian T. Byrnes, David Wands; Phys.Rev. D74 (2006) 043529; DOI: 10.1103/PhysRevD.74.043529; arXiv:astro-ph/0605679v3
- Coles, P., and Lucchin, F. 1995, Cosmology, WILEY, England, UK
- Copeland, E. J., et al. 1994, Phys. Rev. D, 49, 6410

- Dodelson, S. 2003, *Modern Cosmology*, Academic Press, Amsterdam, Netherlands
- Dunkley, J., et al. 2010, astro-ph/1009.0866.
- Georgi, H., Glashow, S. L. 1974, *Phys. Rev. Lett.*, 32, 438
- Gold, B., et al. 2011, *ApJS*, 192, 15
- Graham G. Ross, Gabriel German, J. Alberto Vazquez. *JHEP* 1605 (2016) 010
- Guo Z.-K., D.J. Schwarz and Y.-Z. Zhang. *JCAP* 08 (2011) 031
- Guth, A. H. 1997, *The Inflationary Universe*, Ed. Vintage
- Guth, A. H. 1981, *Phys. Rev. D*, 23, 347
- Hinshaw, G., et al. 2009, *ApJS*, 180, 225
- Hu, W., and Dodelson, S. 2002, *Annu. Rev. Astron. and Astrophys.*, 40, 171
- J.-O. Gong, Multi-field inflation and cosmological perturbations, *Int. J. Mod. Phys.* D26 (2016) 1740003, arXiv: 1606.06971 [gr-qc]
- Keisler, R., et al. 2011, astro-ph/1105.3182
- Kinney, W. H. 2004, CU-TP-1083, astro-ph/0301448
- Kinney, W. H., et al. 2006, *Phys. Rev. D*, 74, 023502
- Kinney, W. H., and Riotto, A., 1998, *Phys. Lett.*, 435B, 272
- Kolb, E. W., Turner, M. S. 1983, *Ann Rev Nucl Part Sci.* 33, 645
- Kolb, E. W., Turner, M.S. 1994, *The Early Universe*, Westview Press
- Komatsu, E., et al. 2009, *ApJS.*, 180, 330
- Komatsu, E., et al. 2011, *Astrophys. J. Suppl.*, 192, 18
- La, D., and Steinhardt, P.J. 1999, *Phys. Rev. D*, 59, 064029
- Larson, D., et al. 2011, *ApJS.*, 192, 16
- Phys. Rev. D* 71 (2005) 063502
- Lewis A., and Bridle, S., 2002, *Phys. Rev D*, 66, 103511
- Liddle, A. 1999, *AIP Conf. Proc.*, 476, 11
- Liddle, A., Mazundar, A., and Schunck, F. E. 1998, *Phys. Rev. D*, 58, 061301
- Liddle, A. 1999, *An introduction to Modern Cosmology*, WILEY, England, UK
- Liddle, A. R., and Lyth, D. H. 2000, *Cosmological inflation and large-scale structure*, Cambridge University Press, Cambridge, UK
- Liddle, A. R., and Lyth, D. H. 2009, *The primordial density perturbation*, Cambridge University Press, Cambridge, UK
- Liddle, A.R. and Lyth, D.H 1992, *Phys. Lett. B*, 291, 39  
arXiv:hep-ph/0210162
- Liddle, A. R., et al. 1994, *Phys. Rev. D*, 50, 12
- Linde, A. D. 1982, *Phys. Lett. B*, 108, 389
- Linde, A. D. 1983, *Phys. Lett. B*, 129, 177
- Linde, A. D. 1990, *Particle Physics and Inflationary Cosmology*, Harwood Academic, Switzerland
- Linde, A. D. 1991, *Phys. Lett. B*, 259, 38
- Linde, A. 2005, *J.Phys.Conf.Ser.*, 24
- Lidsey, J. E., et al. 1997, *Annu. Rev.Mod.Phys.*, 69, 373
- Lyth, D. H., and Riotto, A. 1999, *Physics Reports*, 314, 1
- Lyth, D. H., and Stewart, E. D., 1995, *Physics Rev. Lett.* 75, 201, hep-ph/9502417
- Lyth, D. H., and Stewart, E. D., 1996a, *Physics Rev. D* 53, 1784, hep-ph/9510204
- Mermod P., *Magnetic monopoles at the LHC in the Cosmos*, arXiv:1305.3718
- Mortonson, M. J., Peiris, H.V., and Easther, R. 2011, *Phys.Rev. D*, 83, 043505
- Mukhanov, V. F., and Chibisov, G. V. 1997, *JETP Letters*, 33, 532
- Olive, K. A. 1990, *Physics Reports*, 190, 307
- Padilla, L. E., et al., to be submitted.

- Peiris, H. V., et al. 2003, ApJS., 148, 213
- Planck 2015 results. XI. CMB power spectra, likelihoods, and robustness of parameters, arXiv:1507.02704 [astro-ph.CO]
- Planck 2015 results. XIII. Cosmological parameters, arXiv:1502.01589 [astro-ph.CO]
- Planck 2015 results. XVI. Isotropy and statistics of the CMB, arXiv:1506.07135v2 [astro-ph.CO]
- R. Hlozek., et al. Astrophys. J. 749 (2012) 90
- Riess, A. G., et al. 2009, ApJ., 699, 539
- Riess, Adam G., et al. 2016, astro-ph/1604.01424
- Smooth, G. F., et al. 1992, ApJ Letters, 396, L1
- Springel, V., et al. 2005, Nature, 435, 629
- Starobinsky, A.A (1980), Physics Letters B. 91: 99?102
- Tegmark, M., et al. 2001, Phys. Rev. D, 63, 043007
- The LIGO Scientific Collaboration and The Virgo Collaboration, *A gravitational-wave standard siren measurement of the Hubble constant*
- The Planck Collaboration, 2016, astro-ph/0604069.
- Vilenkin, A., Shellard, E. P. S. 2000, Cosmic Strings and Other Topological Defects, Cambridge University Press, Cambridge, UK
- Vazquez J. Alberto, et al. MNRAS 442:1948-1956, 2012
- Vazquez J. Alberto, et al. JCAP 06 (2012) 006
- Vazquez J. Alberto, et al. JCAP, 08, 001 2013

- J. Alberto Vázquez: Instituto de Ciencias Físicas, Universidad Nacional Autónoma de México, Apdo. Postal 48-3, 62251 Cuernavaca, Morelos, Mexico. (javazquez@icf.unam.mx)
- Luis E. Padilla: Departamento de Física, Centro de Investigación y de Estudios Avanzados del IPN, AP 14-740,07000 México D.F., México. (epadilla@fis.cinvestav.mx)
- Tonatiuh Matos: Departamento de Física, Centro de Investigación y de Estudios Avanzados del IPN, AP 14-740,07000 México D.F., México. (tmatos@fis.cinvestav.mx)